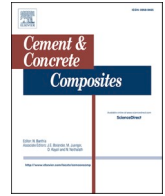




Contents lists available at ScienceDirect

Cement and Concrete Composites

journal homepage: <http://www.elsevier.com/locate/cemconcomp>

CT scanning of internal crack mechanism and strength behavior of cement-fiber-tailings matrix composites

Shuai Cao^{a,b,c,*}, Erol Yilmaz^{d,**}, Zhenyu Yin^{c,***}, Gaili Xue^{a,b}, Weidong Song^{a,b}, Lijuan Sun^e^a State Key Laboratory of High-Efficient Mining and Safety of Metal Mines of Ministry of Education, University of Science and Technology Beijing, Beijing, 100083, China^b School of Civil and Resources Engineering, University of Science and Technology Beijing, Beijing, 100083, China^c Department of Civil and Environmental Engineering, The Hong Kong Polytechnic University, Hung Hom, Kowloon, Hong Kong, China^d Department of Civil Engineering, Geotechnical Division, Recep Tayyip Erdogan University, Fener, Rize, TR53100, Turkey^e State Key Laboratory for Nonlinear Mechanics Institute of Mechanics, Chinese Academy of Science, Beijing, 100190, China

ARTICLE INFO

Keywords:

Cement-fiber-tailings matrix composites
 Polypropylene-polyacrylonitrile fibers
 Industrial computed tomography
 Compressive strength
 Microstructural properties
 3D model reconstruction

ABSTRACT

This paper deals the relationship between compressive strength and internal crack formation (e.g., crack width and volume) of cement-fiber-tailings matrix composites (CFTMC) using an industrial computed tomography system and scanning electron microscopy. Two types of fibers (polypropylene PP and polyacrylonitrile PAN) were used to manufacture CFTMC with a constant cement-to-tailings ratio, solid content and curing time of 1:6, 75 wt% and 14 days, respectively. The results showed that strength gaining of CFTMC increased remarkably with fiber additions which effectively improve its toughness. When compared to samples without fibers, the compressive strength of CFTMC was the highest because of the reduced interconnection between pores and high particle packing density. The internal structure analysis showed that the maximum crack widths of CFTMC increased when the fiber content increased from 0.3 to 0.6 wt%, regardless of fiber type, growing the crack volumes of samples. The failure pattern of all CFTMC samples was mainly tensile, shear and mixed failure (tensile/shear), and a high strength value accompanies with a big volume of crack. At last, the findings of this study may offer a key reference for fiber-reinforced backfills, which can lift their strength, stability and integrity behavior under extreme conditions, such as rock burst, squeezing ground, blast or seismic event.

1. Introduction

The mining sector plays a major role in the economic development of countries but have an adverse impact on ecology and environment by generating the unwanted by-products such as tailings and waste rock [1]. Mineral processing activities can create huge amounts of toxic, corrosive and burnable tailings materials. If released to the environment, these tailings can have major impacts on groundwater, surface water, air and land resources in acidic leachates form [2]. The development and use of underground mineral resources provides a necessary guarantee for human life [3]. However, while human beings are acquiring mineral resources, environmental problems (e.g., groundwater pollution, surface subsidence and collapse of mined-out area)

caused by the mining activities are also becoming steadily prominent [4–6]. Environmental accidents have increased public awareness, and increasingly strict environmental regulations have promoted the research which aims to develop state-of-the-art techniques of eliminating these risks caused by detrimental tailings [7]. The reduction of environmental impacts can be eliminated by best management practices, new legislation and improvements in technology. Backfilling technology offers a smart solution to mines for eliminating the harmful effect of tailings on the environment [8–13]. Hydraulic, rock and paste backfill techniques are considered as main backfilling methods in most mines worldwide [14]. When compared to other types of backfilling, cemented tailings or paste backfill (CTB or CPB) or cement-tailings matrix composites (CTMC) has gained increasing popularity as an

* Corresponding authors. State Key Laboratory of High-Efficient Mining and Safety of Metal Mines of Ministry of Education, University of Science and Technology Beijing, Beijing, 100083, China.

** Corresponding authors.

*** Corresponding authors.

E-mail addresses: sandy_cao@ustb.edu.cn (S. Cao), erol.yilmaz@erdogan.edu.tr (E. Yilmaz), zhenyu.yin@polyu.edu.hk (Z. Yin), hnpyxgl@126.com (G. Xue), songwd2004@126.com (W. Song), sunlj@lnm.imech.ac.cn (L. Sun).

<https://doi.org/10.1016/j.cemconcomp.2020.103865>

Received 30 December 2019; Received in revised form 9 September 2020; Accepted 29 October 2020

Available online 3 November 2020

0958-9465/© 2020 Published by Elsevier Ltd.

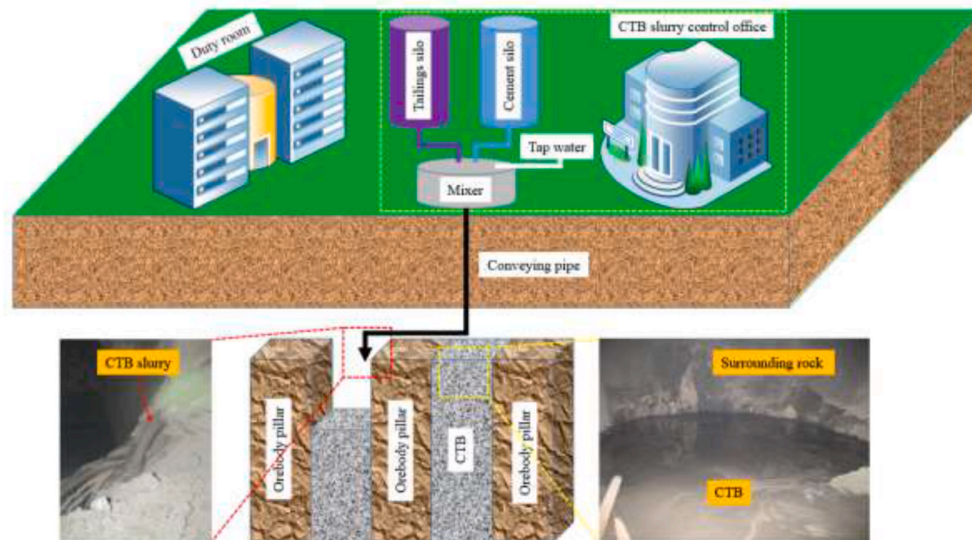


Fig. 1. Backfilling process implemented in underground metal mines.

efficient and effective tailings management for underground mining operations [15–17].

Cement-tailings matrix composites (CTMC) is defined as an engineered, non-Newtonian fluid, and controlled low strength material, which consists typically of processing tailings, hydraulic binder, water, and rarely chemical additives [18–21]. CTMC is manufactured in the surface plant and then transported by gravity or pumping via pipeline to underground mined-out stopes, as shown in Fig. 1. Many studies have been conducted on physical and mechanical characteristics of cemented mine backfill [22–26]. The main factors which greatly affect the quality and performance of the backfill include cement-to-tailings ratio, slurry concentration and curing time [27–29]. CTB contains a small proportion of hydraulic binder (frequently 2–9 wt% by dry mass of mine tailings) and can collapse when subjected to intensive stresses in underground mines [30]. A variety of fibers, which provides a three-dimensional or multidirectional reinforcement throughout the entire concrete matrix, are added to better improve its fresh and hardened properties. Many studies have experimentally shown that, based on its type, length, shape and content, the addition of fiber to concretes and cemented soils can knowingly increase the mechanical strength by help of interlocking of micro-sized grains [31–34]. It should be however kept in mind that there are some differences between those materials and cemented backfills in terms of mineral composition, grain size distribution and filling requirements. To improve the integrity and crack resistance of CTMC, many studies have been undertaken by numerous researchers. Based on the centrifuge model test and limit equilibrium analysis of the stability of mine backfills, Mitchell and Stone [35] pioneered the utilization of fiber on the ultimate backfill design in terms of reducing the cement related costs.

Consoli et al. [36] studied the effect of Portland cement content and dry density on the enhancement of durability and strength of fiber reinforced compacted gold tailings-cement mixes, and found that incorporating fibers can quantify the accumulated loss of mass of fiber-reinforced backfills after wet/dry cycles and result in an increase in compressive strength as a function of the porosity/cement index. Chen et al. [37] conducted an experimental work to research the reinforcement of polypropylene fiber on CPB as a function of cement content, solid concentration, fiber content and fiber length. The results indicated that polypropylene fiber's specific strength when compared with that of samples without fiber is 4 times higher. Besides, the best fiber parameter levels are a fiber content of 0.15% and a fiber length of 6 mm. Yi et al. [38] considered the use of polypropylene fibers to reinforce the partial

or whole body of CPB models in laboratory centrifuge tests. The results showed that the prototype height of fiber reinforced CPB stopes could be much higher than that of unreinforced stopes depending on the extent of reinforcing. Numerous researchers [39–42] reported that the inclusion of fibers help rectify the weakness of non-reinforced fills by mobilizing tensile strength along the failure planes and offered a crack-arresting ability and improved the compressive, flexural, tensile and impact strengths, toughness and ductility. Specially, polypropylene fibers have advantageous of resistance to corrosion and easier dispersion with a backfill matrix than other fibers, such as steel. Addition of fibers to CTB increases the peak strength and decreases its post-peak strength losses. Fibers can be also used for replacing some of the binder used within CTB [43–46].

More recently, Xu et al. [47] have investigated the shear behavior of the interface between granite rock and CPB reinforced with different amounts of fiber (0%, 0.2%, 0.3%, and 0.5% by weight of the total solids). The results indicate that the shear properties and behavior of fiber reinforced CPB-rock interface are a function of fiber content, curing time, pore water chemistry and applied stress. The fiber reinforcement increases the interface peak stress and residual strength up to an optimum fiber content and reduces the contraction at the interface. The degree of vertical deformation also declines with increasing fiber content. To improve the design and optimization of CPB transport systems, Bian et al. [48] studied the effect of sulphate on yield stress and viscosity of fiber reinforced CPB. The results indicate that the yield stress decreases with an increase in the initial sulphate content, while the viscosity increases with increasing sulphate content. The sulphate ions pointedly affect the hydration products that form in the CPB matrix as well as the zeta potential of fiber reinforced CPB material.

The mechanical strength properties of CTB material have been extensively investigated, such as uniaxial compressive strength (UCS), triaxial compressive strength (TCS), flexural strength (FS) and tensile strength (TS), which were closely related to mesoscopic parameters such as internal porosity and crack size [49–52]. To obtain relationships between macroscopic and mesoscopic mechanical properties, non-destructive methods, such as nuclear magnetic resonance [53,54], acoustic emission [55–57] and industrial computerized tomography CT [58–61] were used for characterizing the internal structure of CTB materials. Among other techniques, CT technology has been commonly used for fiber reinforced mortar, cement and concrete investigations [62–66]. An essential advantage of CT scanning technology [67] is that it enables the exact position, and orientation of each individual fiber to

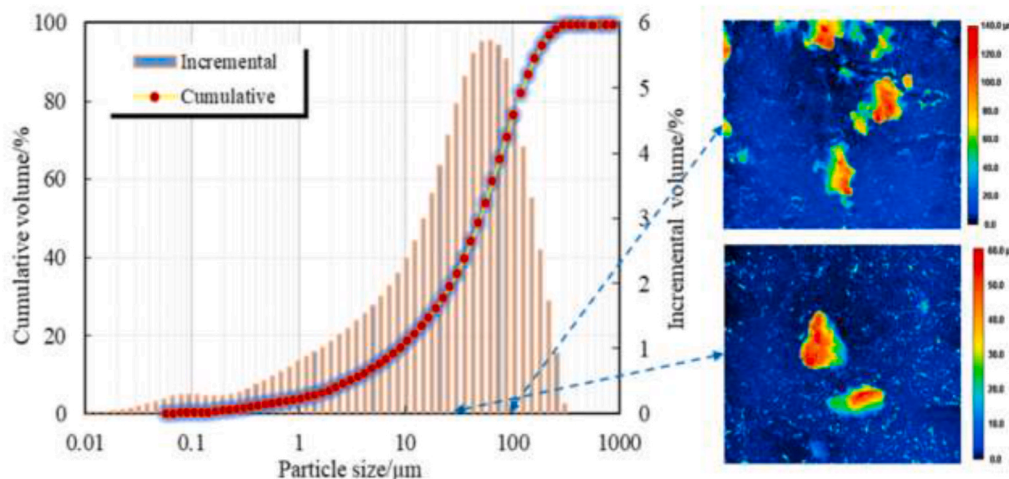


Fig. 2. Grain size distribution curves and 3D laser scanning of gold tailings (modified after [39]).

be measured, which is not possible with other techniques. Chung et al. [68] visualized the spatial distribution of voids on two real cement pastes by means of X-ray CT images and finite element simulation. Mishurova et al. [69] found that CT could be implemented to better analyze the orientation distribution of fibers used within cement-based composites. Indeed, this technique can be used to any kind of composite materials. Yang et al. [70] found that X-ray CT could obtain the information of cracks spatial distribution, gray value, corrosion depth and pore volume distribution. Industrial CT application has advantages in obtaining parameters such as cracks and pores in fiber reinforced composites [71,72]. A full explanation of this technology and its overall use in several engineering areas can be found elsewhere [58,73].

The above studies deliver valuable information and technical data for a better comprehension of the mechanical strength characteristics of fiber reinforced backfills. However, until now, no research has been accomplished on the assessment of an intrinsic relationship between uniaxial compressive strength and porosity of cement-fiber-tailings matrix composites (CFTMC) reinforced with polypropylene (PP) and polyacrylonitrile (PAN) fibers. An in-depth understanding of internal crack mechanism and failure mode of fiber reinforced backfills is critical for assessing their short- and long-term performance. Indeed, the failure mechanisms and models of fiber reinforced backfills clearly exhibit its structural behavior and integrity, which is closely related to higher rigidity, stiffness and strength performance. This study deals internal mechanism (interaction among fiber, cement and tailings) of sliced images acquired from X-ray CT, which may explain the failure behavior as a limitation to crack propagation and extension by the mobilized fiber tensile strength. The ideal types of fibers for the reinforcement of the backfill structures can be determined in terms of strength and ductility, which are two main factors to be considered in the backfill structure design to optimize the economy and safety of mining with backfill. Additionally, the self-supporting capacity of the backfill material with less cement can be improved by implementing fiber technology, thereby reducing the backfill dilution when excavating to adjacent stopes. Hence, a variety of experimental testing which include uniaxial compressive strength, industrial CT system and scanning electron

Table 1

The main chemical composition of gold tailings.

(2) *Binder and water*: Ordinary Portland cement 42.5R as a single binding agent is selected for the preparation of CFTMC samples. The hydraulic cement is typically produced by milling Portland cement clinker together with gypsum. It is classified as OPC 42.5. ‘OPC’ is the symbol for ordinary Portland cement while the number 42.5 shows the minimum desired strength value achieved within 28 days. The chemical composition of the OPC 42.5R is listed in Table 2.

Component (%)	SiO ₂	Al ₂ O ₃	CaO	MgO	P	Fe	S	Au	Ag	Cu
Content	62.77	14.34	1.88	3.38	0.08	2.90	0.15	<0.01	0.032	<0.01

Table 2

The main chemical composition of the cement OPC 42.5R

Chemical composition	SiO ₂	Fe ₂ O ₃	Al ₂ O ₃	MgO	CaO	SO ₃	K ₂ O
Content (%)	20.1	2.91	5.11	1.57	61.8	1.98	0.37

microscopy are conducted in this study to better understand this internal structure behavior. The main objectives of this study are: i) to analyze the real structure of CFTMC by using 3D reconstruction technology; ii) to assess the relationship between strength and microstructure of CFTMC samples; and iii) to develop a good understanding of the failure behavior of CFTMC.

The outline of this study will be as follows: the experimental program will be given in Section 2, the results and discussion will be presented in Section 3, describing the relationship between strength and microstructure of CFTMC, and eventually, the conclusions will be presented in Section 4.

2. Materials and methods

2.1. Experimental materials

The CFTMC samples were prepared by mixing gold tailings, cement, fibers, and mixing water. The parameters of each experimental material were given in detail as follows.

- (1) *Gold tailings*: The gold tailings material used in this study is sampled from a gold mine located in Shandong, China. The grain size distribution curves of gold tailings are shown in Fig. 2. For the soil material to be well graded the value of coefficient of uniformity C_u must be greater than 4 and the value of coefficient of curvature C_c should be in the range of 1–3 [74]. The C_u and C_c values of gold tailings samples are 15.63 and 1.84, respectively. The quantity of particles finer than 20 μm in size was 19.5 wt%, showing a good ability to retain enough water to form the paste material. The sampled tailings can be categorized as

Table 3

The main chemical composition of tap water used as mixing water.

(3) *Fibers*: According to ASTM and ACI standards [76,77], fibers are divided into four categories, based on the type of material from which the fiber is produced. In this study, Type III – synthetic fiber is used as polypropylene (PP) and polyacrylonitrile (PAN) fibers. Synthetic fibers are the most widely used type of fiber and may be classified as microfibers or macrofibers [77]. The basic parameters of these two fibers are listed in Table 4. The importance of the interaction between fibers and the cement matrix has been found to be a critical parameter in the composite performance, which led to interface modification techniques to achieve the desired properties.

Varieties	Conductivity	pH	Chloride	Aluminum	Sulfate	Sodium	Iron
	121.5 $\mu\text{S}/\text{cm}$	7.35	5.69 mg/L	4.32 $\mu\text{g}/\text{L}$	4.62 mg/L	7.84 mg/L	2.36 $\mu\text{g}/\text{L}$

Table 4

Basic parameters of the synthetic fibers used in the experiments.

Fiber type	Length (mm)	Density (g/m^3)	Tensile strength (MPa)	Young's modulus (GPa)	Elongation rate (%)
PP	12	0.91	398	3.85	28.0
PAN	12	0.91	736	4.68	30.0

Table 5

Mixture proportions of CFTMC samples used in the experiments.

Specimen ID	Cement (kg/m^3)	Water (kg/m^3)	Tailings (kg/m^3)	Fiber content (kg/m^3)
N-1:6	210	490	1260	0
PP-0.3	210	490	1260	4.41
PP-0.6	210	490	1260	8.82
PAN-0.3	210	490	1260	4.41
PAN-0.6	210	490	1260	8.82

coarse-grained according to the Canadian mine tailings classification system [75].

Table 1 lists the chemical composition measurement results (XRF) of the studied gold tailings, from which one can observe that the content of SiO_2 is 62.77%, and the total content of main oxides (Al_2O_3 , SiO_2 , MgO , and CaO) amounts to 82.37%.

Mixing water can greatly affect the backfill strength as a function of the water-to-cement ratio and cement hydration mechanism [14]. In this study, tap water was used as mixing water to homogeneously mix solid materials. Table 3 lists the chemical composition of tap water.

2.2. Preparation of CFTMC samples

In this study, the value of curing age, solid content and cement-to-tailings ratio of the manufactured CFTMC samples was constantly set to 14 days, 75 wt%, and 1:6, respectively. Synthetic PP and PAN fibers were selected as additive materials. The fiber contents were also set to 0% (control), 0.3%, and 0.6% by the total mass of tailings and cement, respectively. The method used for the addition of fibers is crucial in delivering consistent and homogeneous fiber reinforced backfills and to prevent or significantly minimize balling. Fibers should not be loaded in the batching sequence with the cement. Instead, they should be loaded at the same time as the coarse aggregates in order to take advantage of the shear that the aggregates provide. If that is not possible, they may be loaded up front with the head water, with the mixer turning at slow speeds. A final option would be introducing them after the batching cycle has been completed. Mixing time will vary based on when the fibers are introduced into the mixture and normally ranges from 3 to 5 min. It should be noted that longer mixing time is preferred when the fibers are added after all the standard ingredients have already been introduced and mixed. Additional attention must be given to the backfill mixtures with low slump. The poor workability mixtures are generally not preferred in fiber reinforced backfills as they may lead to non-homogeneous fiber distribution. In this study, tailings, cement and

fiber in a dry state were concurrently mixed and stirred for 3 min. Then, quantitative tap water was added, as stated by the ASTM and ACI standards [76–78] and stirred for 3 min until the CFTMC slurry becomes homogeneous (i.e., particles distributed uniformly). Besides, the calculation (calculated by mass fraction) of the proportions of each sample is listed in Table 5. Note that a high-precision electronic scale an accuracy of 0.01 g was used to weigh the sample ingredients. All samples were clearly numbered in the form of ‘fiber type-fiber content’. For example, PP-0.3 represents a CFTMC specimen having a PP fiber content of 0.3%.

In this study, cylindrical molds were chosen to prepare a number of CFTMC samples, which were molded 50 mm in diameter and 100 mm in height. To facilitate demolding, peanut oil was wiped into the inner wall of molds in advance. CFTMC slurry was poured into these cylindrical molds and then the prepared samples were placed into a curing box having a temperature of 20 ± 1 °C and a humidity of 95% during the curing process. The demolding time was set 2 days based on experimental experience [68]. All CFTMC samples were cured in the same curing condition for 14 days until the test duration. It is well-known that the backfill is an integral part of production cycle at most modern mine sites worldwide. An ongoing quality control/quality assurance (QC/QA) test program is crucial to ensure that the desired backfill strengths are achieved, at acceptable cement contents, without endangering the overall security of underground mining structures and operations. A curing time of 28 days, which allows the backfill matrix to sufficiently cure and reach a minimum compressive strength in order to ensure the safety of the workers and the safe extraction of the ores in the neighbor stopes of the backfilled area, are most often considered as part of a routine QC/QA test program in mines. However, the time is so critical in the mining industry, and as the mining cycle becomes shorter production increases significantly. Experiences show that, in the backfill mix made with fiber and OPC 42.5R cement, the cement hydration process starts abruptly, and strength gain begins immediately after final set. Accordingly, a 14-day curing time becomes sufficient for the backfill matrix which results in an equal or even more rapid gain in the strength. Additionally, Ranade et al. [50] suggested that the compressive strength evolution of the samples cured using the given 14-day curing regime is equivalent to the strength evolution of the 90-day samples cured in ambient conditions. At the end of 14-day curing regime, the surfaces of samples were ground flat for UCS testing.

2.3. Experimental procedures

2.3.1. Uniaxial compressive strength tests

Various uniaxial compressive strength (UCS) tests were conducted on CFTMC samples according to the ASTM C39 standard [79]. A microcomputer controlled electronic universal testing machine with a maximum capacity of 100 kN was used for UCS testing. The loading rate was set to 0.5 mm/min in this study in accordance with the GB/T17671-1999 standard method [40]. A computer acquisition system was able to record the load and displacement data during the whole loading process. Axial loading was automatically terminated when the tested sample developed a clear shearing plane and peak strength had been mobilized. At least three CFTMC samples for each group were carried out in the laboratory, and the average UCS value was considered in the present study.

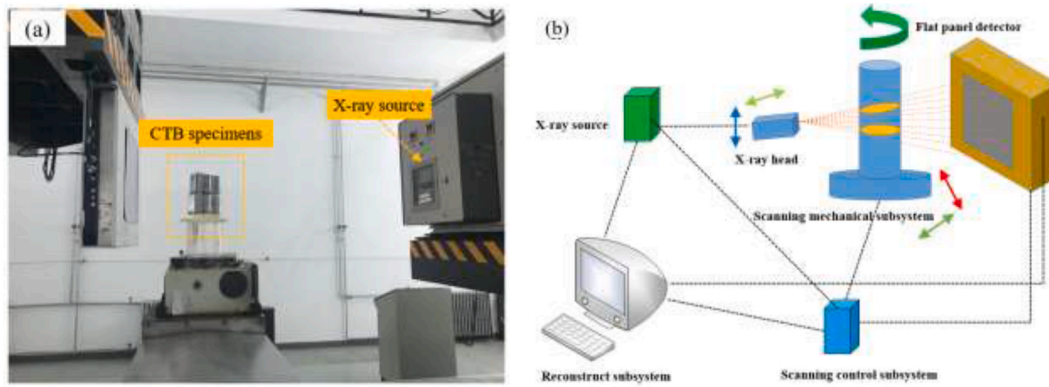


Fig. 3. Industrial CT scanner: (a) schematic diagram and (b) its working principle.

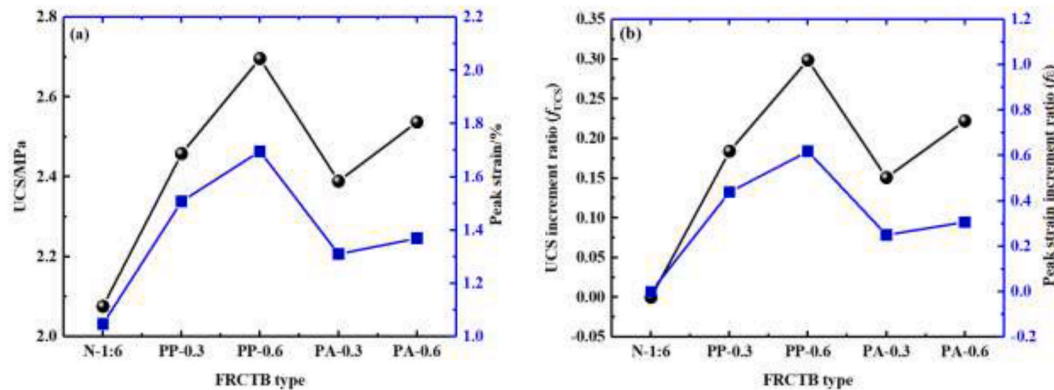


Fig. 4. Relations among UCS and CFTMC type: a) peak strain; and b) peak strain increment.

2.3.2. X-ray computed tomography

Industrial CT is a non-destructive system used to study the internal structure of materials, adopting the principle of X-ray radiation imaging [80–83]. The CT scan system, as shown in Fig. 3, integrates an intensity-controlled X-ray source and a detector, which measures the loss of X-ray intensity. X-rays are emitted during scanning while a detector measures and records the final X-ray intensity for all X-rays. Rotating samples under test, many relative directions across sample are applied and, eventually, every point of sample is traversed by different X-rays, from different directions. Industrial CT system provides cross-section images, and it shows the internal structure of workpiece, density distribution, and defects location. The sharpness of the 2D image acquired by the industrial CT and the reconstructed 3D image was closely related to the energy of X-ray. Generally, the higher the X-ray energy, the clearer the image acquired. The X-ray energy and spatial resolution were set as 6 MeV and 2.5 LP/mm, respectively. Also, the environmental temperature and density resolution were set as 25 °C and 0.5%.

2.3.3. Scanning electron microscopy

Scanning electron microscopy with energy dispersive X-ray spectroscopy (SEM/EDX) was used to observe the interaction between fibers and CFTMC. SEM tests were completed by using a Carl Zeiss Evo®18 apparatus with a resolution of 1.0 nm and an accelerating voltage of 30 kV. The X-ray detector used for the EDX analyses was an Oxford X-Max 50 detector with a resolution of 125 eV on the manganese K_{α} line. The SEM image pixel size was 1024×768 [84]. Initially, SEM samples were obtained by cutting the middle part of CFTMC. Before SEM tests, the surfaces of samples need to be dried first and then carbonized after the first step [85].

3. Results and discussion

3.1. Mechanical properties of CFTMC samples

Fig. 4 shows the relationship between compressive strength and CFTMC sample types. It is clear that the mechanical strength properties are improved when fibers, regardless of their types, are added to the cement-tailings backfill matrix. Among others, the highest strength values of PP fiber-reinforced samples were found to be 2.5 and 2.7 MPa for a fiber content of 0.3 and 0.6 wt%, respectively. PP fibers are easy to split into finer sizes and durable in the environment of the backfill matrix in comparison with PAN fibers. PP fibers also provide a relatively high elastic modulus and strong bond when a sufficiently large volume of fibers is used. In this case, a fiber content of 0.6 wt% is sufficient for UCS improvement.

Additionally, Fig. 4a directly describes the relationship between compressive strength and CFTMC type. One can say that the strength values of CFTMC samples with PP and PAN fibers are significantly different. When compared with non-cement-fiber-tailing matrix composites (NCFTMC), the compressive strength of all kinds of CFTMC is larger than samples with fiber reinforcement. The results also show that compressive strength of the PP CFTMC with a fiber content of 0.6 wt% is the highest, reaching 2.7 MPa, which is 29.8% higher than that of NCFTMC samples. When the fiber content in the matrix was 0.3 and 0.6 wt%, the corresponding strengths were 2.39 and 2.54 MPa, respectively. Besides, the UCS increment was 15.1% and 22.2%, respectively. Fig. 4b also shows the relationship among UCS, peak increment and CFTMC type. One can observe from the peak strain characterization of CFTMC and NCFTMC samples that the peak strain of CFTMC was significantly larger than that of NCFTMC. When the fiber content was 0.3 wt% and 0.6 wt%, the peak strain values of CFTMC samples reinforced with PP

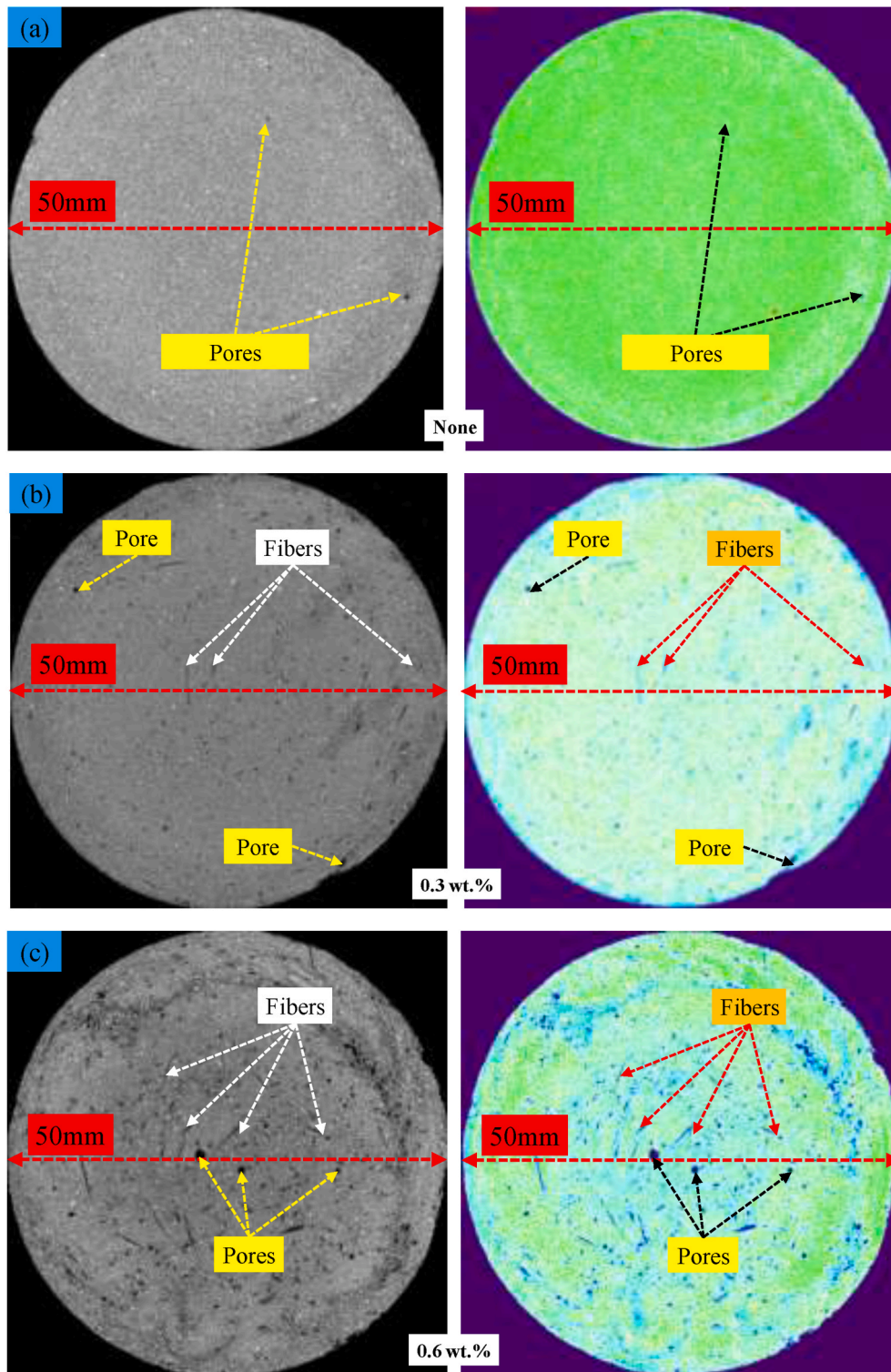


Fig. 5. 2D raw and processed images of CFTMC samples: a) None; b) 0.3 wt%; and c) 0.6 wt%.

and PAN fibers were 1.51%, 1.70%, 1.31%, and 1.37%, respectively. The corresponding peak strain increments were 43.8%, 61.8%, 25%, and 30.6%. Consequently, the toughness of CFTMC can be effectively improved by adding fiber. This can be attributed to the supplementary contribution of the tensile strength of fibers at higher strain values. The strength gain of non-reinforced samples was mainly because of the hydration products, which form a bonding effect. The bonds between particles in the backfill matrix with relatively lower cement amount

were easier to break. However, fiber reinforcement allows solid particles to act in union, which provides further resistance to failure as they tend to have both high strength, and significant deformation before failure. Besides, fiber-reinforced sample provides a significant increase in its ductility behavior mainly due to the mobilization of resisting forces by fibers crossing developing failure planes. Fiber inclusion enhances a particle-fiber interaction, with the fibers interlocking with cementitious mass as the tensile strength of fibers is mobilized.

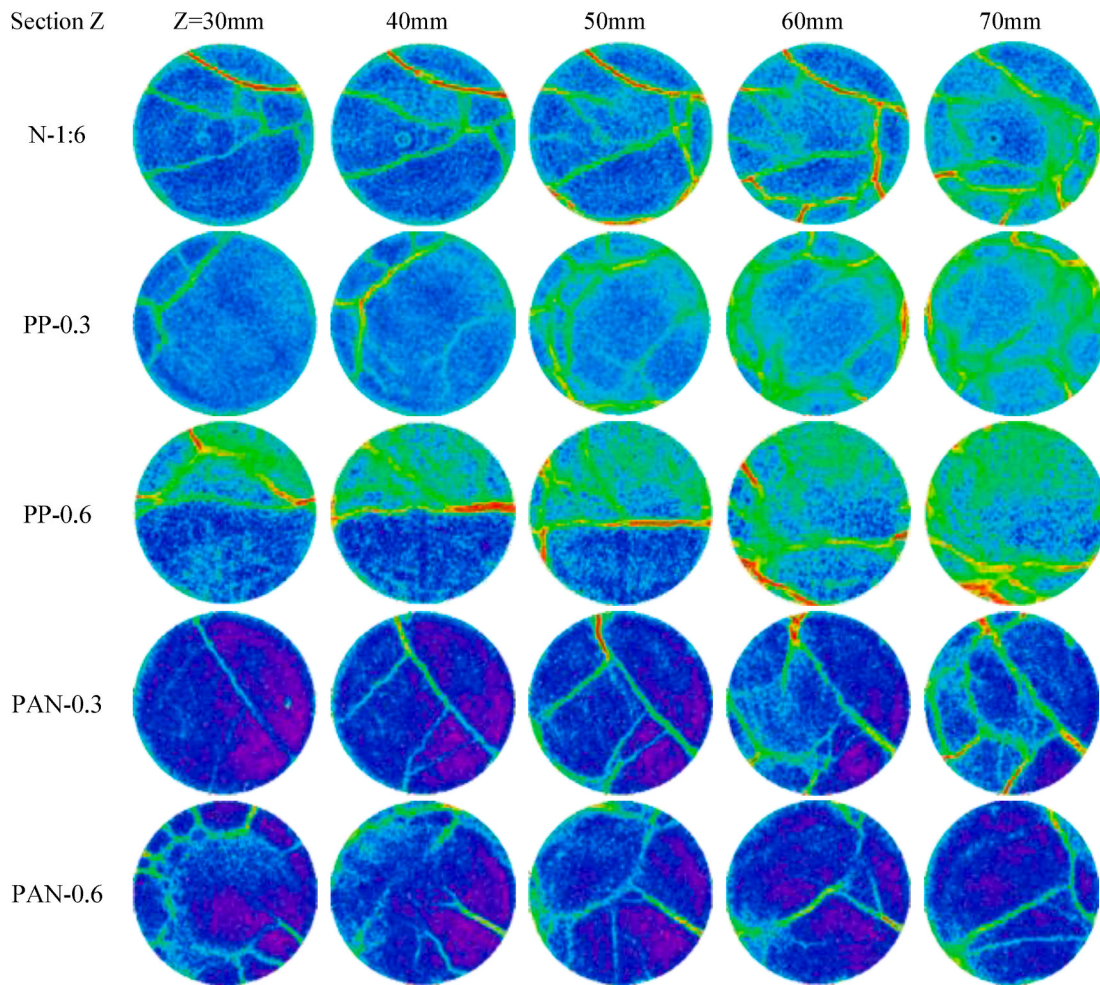


Fig. 6. 2D proceed cracks images of samples with and without fiber reinforcement.

3.2. Industrial CT scanning analysis

3.2.1. 2D pore structure of pre-load CFTMC

Industrial CT was used to study the pore and crack sizes in 2D images. Fig. 5 demonstrates the raw and processed images of samples reinforced with and without fiber. One can observe from these images that the fiber distribution within CFTMC samples is relatively uniform, indicating that the mixing process is well done during the preparation of the tested samples. The main problem was small size relative to the resolution of the phases that were too similar to one another to easily separate. However, the existence of fiber within CFTMC with a fiber content of 0.6 wt% are easily recognized in Fig. 5c. There were unfilled spaces (air or water filled porosity) as well as fiber phases in the proceed 2D images.

Fig. 5 also shows a typical sample scan of samples, in which four different phases (e.g., unreacted cement grains, inner C-S-H gels, calcium hydroxide and unfilled spaces) can be identified by using X-ray CT. It is clear that non-reinforced sample is dominated by the C-S-H gel, whereas samples with fiber have little C-S-H present. This difference is most likely as a result of different setting times used for cement. The densest phase is linked with fiber reinforced samples where fibers are interlocked with particles, delivering the strength to stop grains from segregating and thus deferring the failure of samples.

3.2.2. 2D crack structure of CFTMC after loading

The 2D images of CFTMC samples were obtained by the slicing function of industrial CT, and 100 slices were obtained with 1 mm spacing along the Z-direction of samples [86]. 2D sections with interface

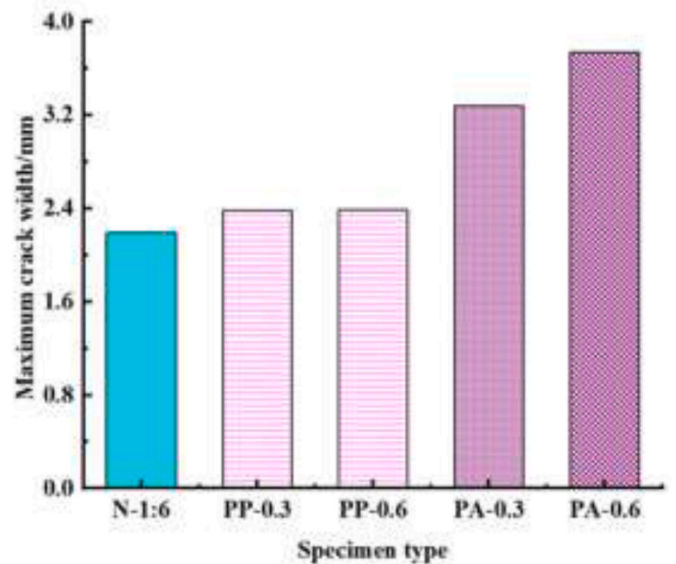


Fig. 7. Maximum crack width of CFTMC and NCFTMC samples.

heights of 30, 40, 50, 60 and 70 mm were selected to study the crack properties of CFTMC. The Image J software was used to analyze the crack sizes. A pseudo color enhancing algorithm was used to process the

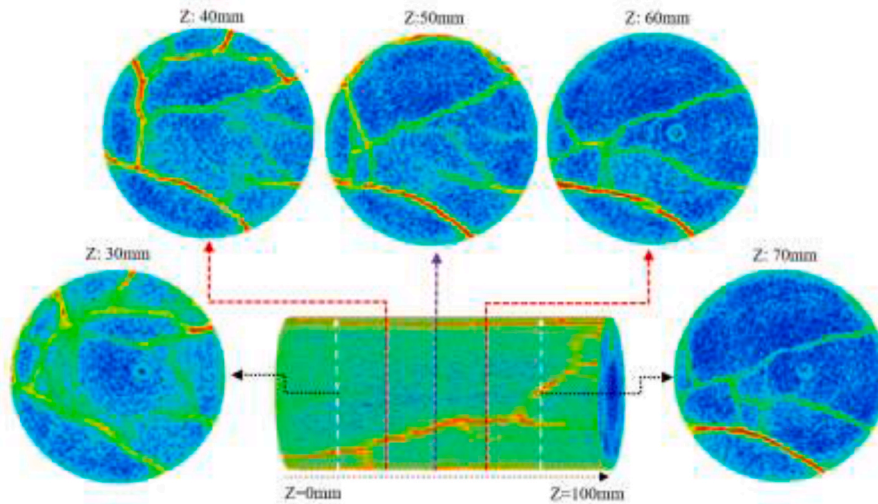


Fig. 8. The process of 3D reconstruction model of NCFTMC samples.

original images to compare the differences from the CT images [87]. Fig. 6 demonstrates the 2D images of both NCFTMC and CFTMC samples.

One can say that different colors represent different objects. Taking N-1:6 sample as an example, the red and green colors mean the cracks in each cross-section. The red color indicates that the depth of the crack is deeper than the green one. From Fig. 6, it can be seen that samples contain pore structures, and crack initiation and expansion occur in the area with concentrated tensile stress on the periphery of pore space when the backfill matrix is subjected to external loads. This continues until fill fails. The number of high-density areas in CT images increases with increasing fiber content (0.6 wt%). At the same time, the pore spaces increase evenly. The major cracks of non-reinforced samples spread from the top to the bottom of sample whereas fiber reinforced samples curb the growth of cracks by the bridging effect of fibers, and the failures occur through the development of irregular gaps at the edge of samples.

Fig. 7 shows a histogram graph of sample type and maximum crack width for diverse fiber reinforced samples. The maximum crack widths of PP-0.3 and PP-0.6 are 2.38 mm and 2.39 mm, respectively. Note that the maximum crack width of the sample N-1:6 is 2.19 mm. At the same time, the maximum crack widths of the samples PAN-0.3 and PAN-0.6 are 3.28 mm and 3.74 mm, respectively. In addition, one can state that the maximum crack widths of the tested samples increase when the fiber content increases from 0.3 to 0.6 wt%, regardless of PP or PAN fiber. Why this happens? We analyzed the results obtained in this study, and the fiber quality used in this laboratory was poor. As we know, the traditional fibers are not hydrophilic. However, as shown in Fig. 12 and Fig. 13, the scanning electron microscopy results show that the fibers have agglomerated and cracked in this experiment. Due to fiber cracking and deformation, the maximum crack width and total volume with more fiber content also become larger. Especially the fiber content is more obvious at 0.6 wt % than 0.3 wt %. Thus, the fiber clumping and cracking may be the main reason for the increase in crack width and total volume. Besides, we also found that the failure modes of cement-fiber-tailings matrix composites (CFTMC) are so different from the fiber reinforced concrete. Because concrete specimens developed later expansion and gradually generated micro cracks in the weakest zone with increasing compression loads. Fibers began to be stretched and debonded at fiber-matrix interfaces when these cracks reached fibers. The processes reduced crack-tip stress concentration by fiber acting as stress-transfer bridges [94]. Moreover, the particle distribution of concrete is also so different from the CFTMC. The tailings gradation is finer than that of concrete. The bridging effect of fiber in concrete is more

significant than CFTMC. The possible reason the stretching ability is mainly rely on the friction between fibers and matrix when the crack extends to the fiber-matrix interface. Banthia et al. [95] found that a well-bonded cellulose fiber presumably fractures across a matrix crack and fails to provide post-crack ductility. However, we also found that the fibers are pulled out instead of being broken. The crack width continues to expand, but the fiber can still stretch the segments. Note that PP fiber reinforced samples maintained their integrity by the application of load in the strength tests, contrary to PA fiber reinforced samples that exhibited significant spalling during testing. This indicates to the potentially beneficial effect of PP fibers in improving the ductility of the backfill matrix.

3.2.3. 3D structure reconstruction

The uniaxial compression test only provides parameters such as its compressive strength and elastic modulus. However, it is impossible to explain the reasons for the differences observed in the mechanical strength of samples. Since the CT two-dimensional images can only reflect limited information, the theory of 3D reconstruction was introduced for the reconstruction of CT images. The data obtained from industrial CT scanning was imported into image J software for three-dimensional reconstruction of pores and cracks in the tested samples. After this, the volume of pores and cracks were quantitatively analyzed. In this study, the samples N-1:6, PP-0.3, PP-0.6, PAN-0.3, and PAN-0.6 were scanned thoroughly. The 100 slices of 2D images were obtained from each of these five samples [88]. Firstly, all these 2D images were imported into Image J software by using the “file → import → import sequence function”. Secondly, these images should be converted to 8 bits type. Thirdly, the “Plugins → 3D → Volume Viewer” function was used to reconstruct the 3D model [89]. Taking the sample N-1:6 as an example, the process of the 3D reconstruction is shown in Fig. 8. Note that the division and extraction of different components had a major impact on subsequent 3D reconstruction of samples, as inappropriate division can cause an error in the reconstructed results.

In addition, Fig. 9 shows a 3D reconstruction of five kinds of CFTMC samples. The models were screened by rotating 90° along the Z-axis to obtain 3D model drawings of 0°, 90°, 180°, and 270°. One can articulate from Fig. 9 that the locations of cracks and failure pattern can be easily obtained accurately. The failure pattern of samples with and without fiber reinforcement is mainly tensile, shear and mixed failure. PP and PAN fibers have an important influence on failure pattern of CFTMC samples. The fibers can efficiently limit crack propagation and improve the toughness. After the compressive destruction, some small cracks appeared on surface of fiber reinforced samples. However, they retain

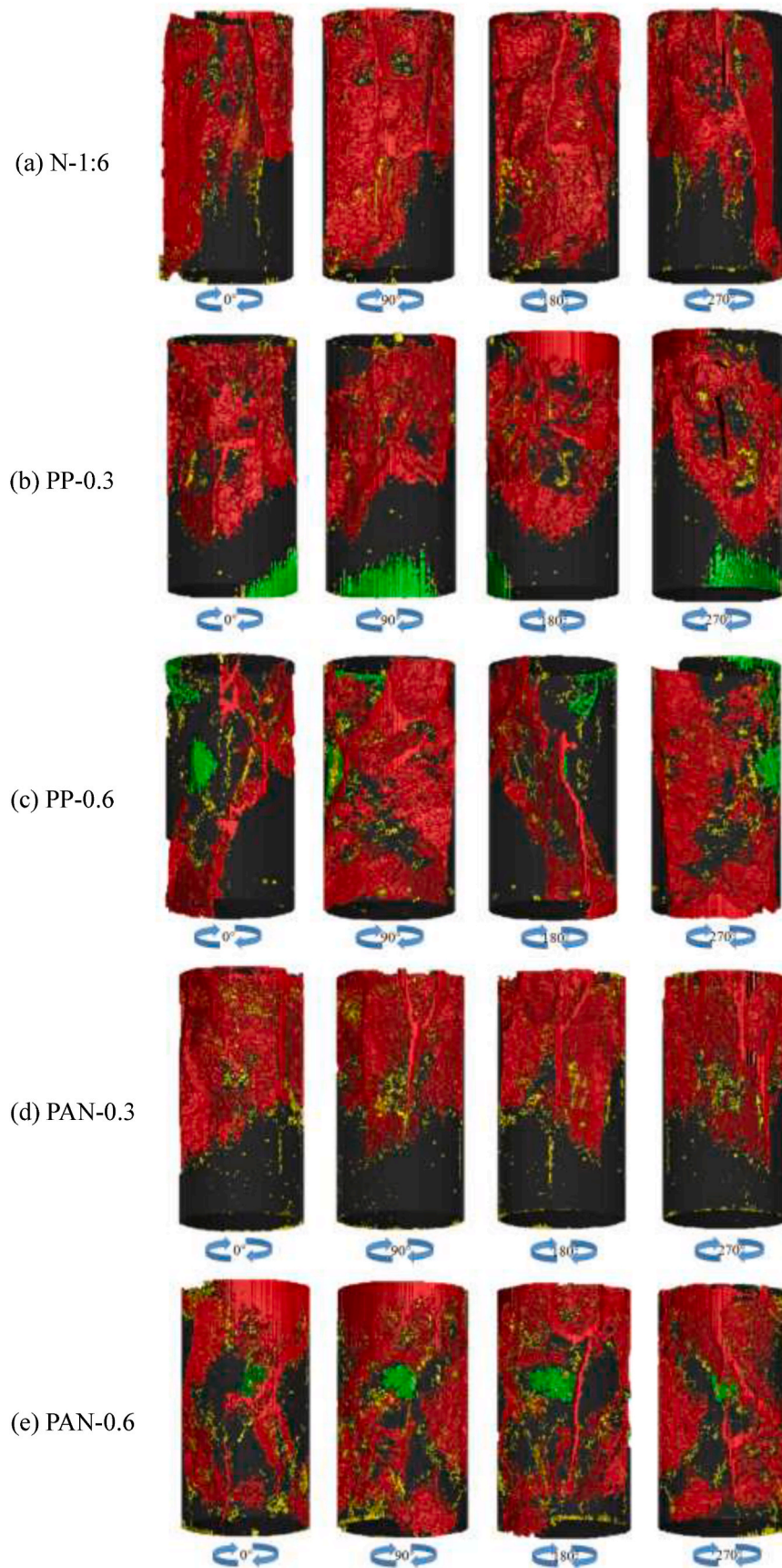


Fig. 9. 3D reconstruction model of both NCFTMC and CFTMC samples.

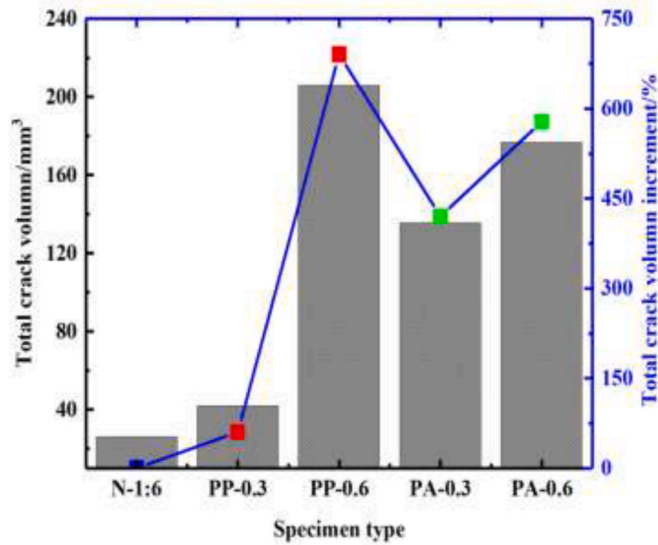


Fig. 10. Relations among specimen type, total crack volume and total crack volume increment.

the structural integrity and residual strength even if the ultimate compressive strength is exceeded. Non-reinforced samples present some large cracks and fracture zones under compression. It should be kept in mind that fibers are inclined to bridge the cracks and stop crack propagation, thereby preventing premature failure and improving the strength and stability of the studied samples.

Fig. 10 analyzes the relationships between the sample type and the total crack volume and the total volume increment of crack. The total crack volumes of N-1:6, PP-0.3, PP-0.6, PAN-0.3, and PAN-0.6 are 26.1 mm³, 41.8 mm³, 206 mm³, 135.7 mm³, and 176.9 mm³, respectively. When compared to the sample N-1:6, the total crack volume increment of PP-0.3, PP-0.6, PAN-0.3, and PAN-0.6 are 60.2%, 690.6%, 420.3%

and 578.5%, respectively. The volumes of fiber reinforced samples are much larger than those of non-reinforced ones right after the end of loading. It can be also found that the effect of PP fibers is more sensitive to PAN fibers on the total crack volume.

As the fiber content in cementitious fill matrix increases from 0.3 to 0.6 wt%, the total crack volumes of the corresponding tested samples increase. It has been experimentally showed that, under the loading condition, the fiber can effectively prevent the falling of the CFTMC block from the tested samples. The crack propagation absorbs more energy, which explains the fact that the higher the fiber content is, the higher the compressive strength is for a given fiber reinforced backfill recipe. This because of a strong structure in the interior of fiber reinforced backfill. When samples are subjected to external compression, strong structure surfaces result in a remarkable increase in the strength development of samples.

3.3. Relation between UCS and microstructures

Pore structure is a vital microstructural characteristic of a porous matrix, as it affects the physical and mechanical properties and controls the durability of cementitious materials such as CTB. The behavior of a porous material is strongly affected by the distribution of pores of various sizes within the solid. Pore size distribution (PSD) is affected by the tailings grain size and packing. The detailed characterization of the pore structure (e.g., total porosity, macro-pores, meso-pores, PSD, threshold diameter and critical pore diameter) of cementitious backfill materials is complicated by the presence of pores having different shapes and sizes and by the connectivity between pores.

To illustrate the internal relationship between compressive strength and macroscopic crack, Fig. 11 was plotted according to experimental results. As can be seen clearly from Fig. 11, the larger the strength values of the tested specimens, the larger the corresponding total volume. The reason is that the expansion of the internal crack of the tested specimen needs to absorb energy, and the incorporation of the fiber just creates conditions to absorb energy. The similar test results can be found in ultra-high-performance fiber reinforced concrete materials, the addition

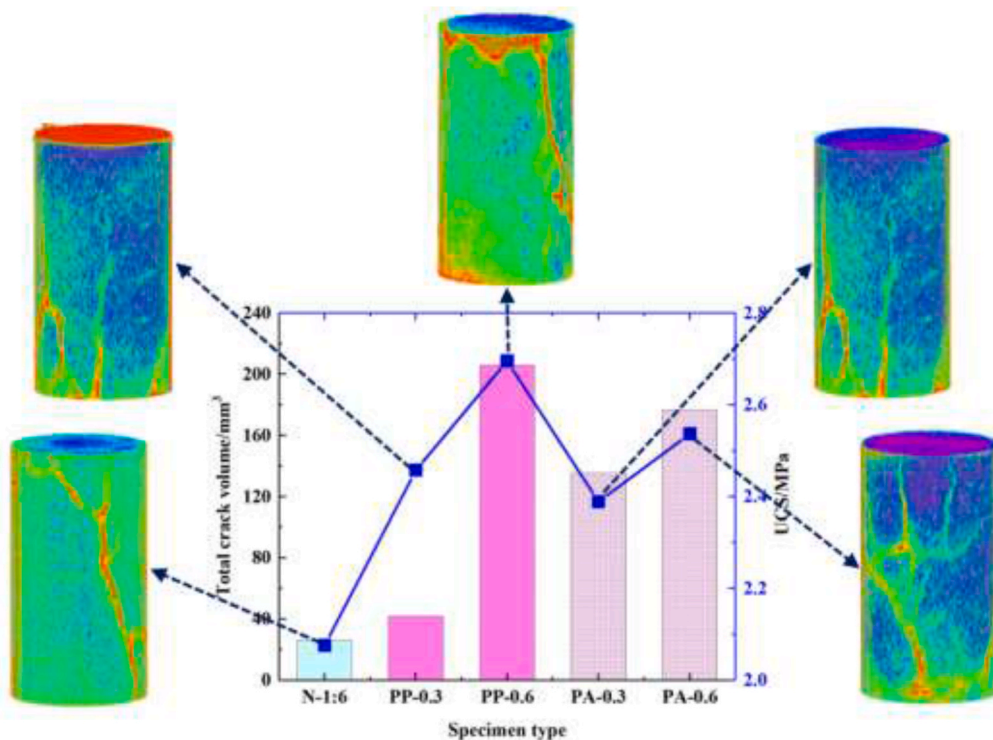


Fig. 11. Relationship between specimen type and total crack volume of tested specimens.

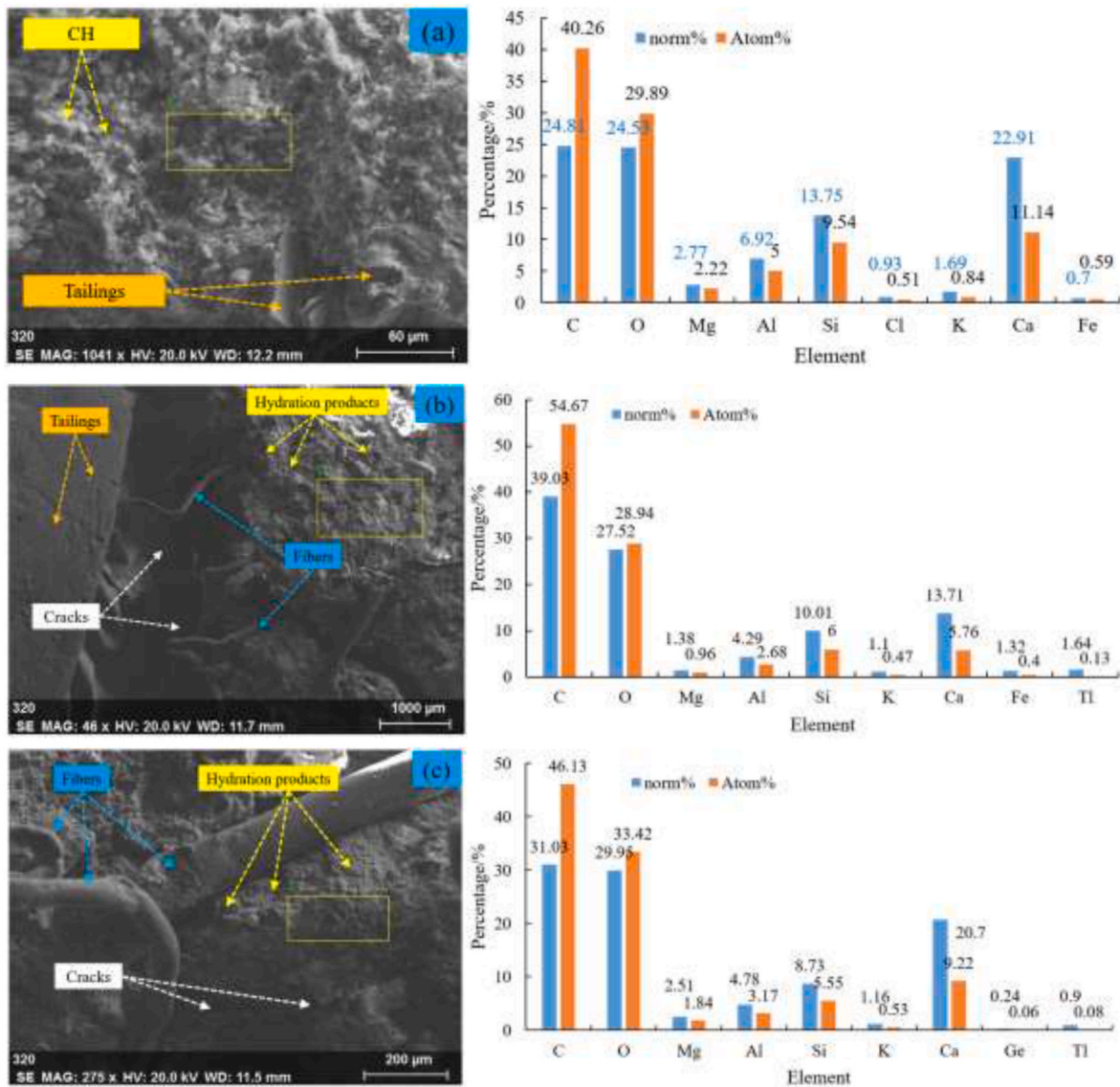


Fig. 12. SEM-EDX results of NCFTMC and CFTMC samples: a) N-1:6; b) PP-0.3; c) PAN-0.3.

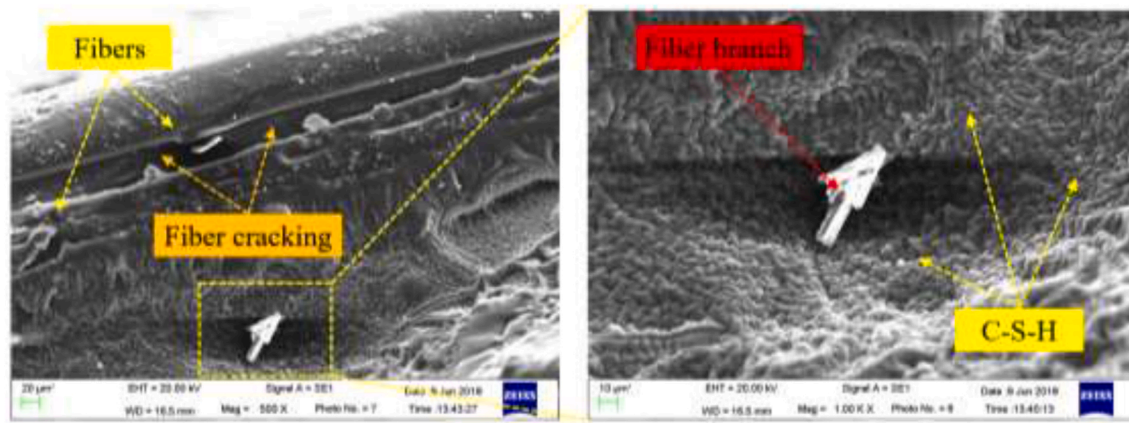


Fig. 13. SEM observations of CFTMC samples.

of fiber to cementitious materials can effectively improve the energy absorption capacity [90]. A strong bonding quality between the fibers and the matrix makes strong interfacial regions that result in debonding

and frictional pullout of fiber packs. Inhibiting the ductile deformation and mobility of the matrix, this failure mechanism clearly lowers the ability of the composite system to absorb energy during fracture

propagation.

3.4. Micro-structural characteristics of CFTMC samples

The SEM method supplies a good platform to study the microstructures of cementitious materials [91]. In this study, the SEM micrographs of different CFTMC and NCFTMC specimens at 14 days were presented in Fig. 12. The tested backfill samples were selected from the failure of CFTMC samples after UCS testing. Fig. 12a shows the microstructure of N-1:6 samples, the elements of hydration product are mainly C, O, Si and Ca, and the content of the above elements is 90.83%. Additionally, the hydration products of samples without fiber reinforcement include calcium silicate hydrate (C–S–H) gel and calcium hydroxide (CH) crystals [92,93]. Figs. 12b and c reveal the SEM micrographs (equipped with EDX analysis) of the samples PP-0.3 and PAN-0.3.

Additionally, the interaction of PP fiber with tailings particles and cement is much better than that of PAN fiber since the high fracture strength and elastic modulus of PP fiber offer a strong flexibility. Under compression, the fiber provides elastic deformation without breaking. Later on, some fibers were pulled out after preventing the destruction of the matrix. Some fibers were wrapped in particle-cement matrix under the action of high viscosity while others display that C–S–H gels are trapped on surface of PP fibers. This eventually results in an increase in the strength of PP fiber reinforced samples.

Fig. 13 also shows that both PP and PAN fibers do not participate in the hydration due to its stable chemical properties, as experimentally demonstrated previously by Xu et al. [29]. The main function of fibers is to connect the hydration products. PP fiber can be effectively combined with the backfill matrix. The fibers eventually act as the bridge among the backfill matrix microstructures, thereby controlling the crack development and permitting fiber reinforced samples to endure a higher peak stress. It is also clear that particles, C–S–H gels and fibers form a whole and denser structure. In some part of fibers that were pulled out, a certain amount of C–S–H gels remains trapped on surface of the fiber. One can also observe that there were pointedly denser the C–S–H gels within fiber reinforced samples.

Moreover, it is also found that the section of the fiber is not originally cylindrical, some part of fibers' cross-sections become elliptical. Some of the fibers have been bent apparently. This is because the fibers are pulled out due to the crack propagation during the loading process. In other words, the tested CFTMC sample consumes more energy during loading mainly due to the fiber being stretched. This also explains why the compressive strength of CFTMC is higher than that of sample without fiber.

4. Conclusions

To investigate the relationships between internal structure, crack mechanisms and macro strength of CFTMC, uniaxial compressive, industrial CT scanning and scanning electron microscope measurements were taken on CFTMC samples with different *c/t* values. For comparison, NCFTMC samples were also prepared. Based on the performed experimental results, the following conclusions can be made:

o The strength performance of CFTMC samples increased as the fiber content increased from 0 to 0.6%. When compared to samples without fiber reinforcement, the strength performance of all kinds of CFTMC samples is larger than non-reinforced samples. Apparently, the addition of fiber can effectively improve the ductility of CFTMC samples.

o The maximum crack widths of the tested CFTMC samples increase remarkably when the fiber content increases from 0.3 to 0.6 wt%, regardless of either PP or PAN fiber. As the fiber content in the backfill matrix increases from 0.3 to 0.6 wt%, the total crack volumes of the corresponding tested samples also increase proportionally.

o The failure pattern of both NCFTMC and CFTMC samples is mainly tensile, shear and mixed failure (e.g., tensile and shear). One can comment that the higher the strength performance of the tested CFTMC

samples, the larger the corresponding total volume.

The CT scanning device offers a massive amount of useful information. However, it is not possible to obtain conclusions through the direct observation of 3D images alone. The data must be post-processed by using a digital image processing software, as preliminarily presented in this study. Based on this, the influencing mechanism of different fiber types and contents on mechanical strength properties from the perspective of energy dissipation could be studied effectively. The damage constitutive model of CFTMC under compression can also be established. Further investigations should be conducted the effect of fiber types and contents on quality and performance of the backfill matrix by focusing on the reduction of the financial costs by significantly reducing the cement expenses. As a result, the findings of this study may give a reference for the macroscopic and mesoscopic mechanics of the backfill matrix.

Declaration of competing interest

The authors declare that they have no known competing financial interests or personal relationships that could have appeared to influence the work reported in this paper.

Acknowledgements

This work was financially supported by the National Natural Science Foundation of China (Grant No. 51804017), the Opening Fund of State Key Laboratory of Nonlinear Mechanics (Grant No. LNM202009) and the Fundamental Research Funds for Central Universities (Grant No. FRF-TP-20-001A2). Special thanks are extended to Shuai Zhou from GRANPECT company limited for his technical help.

References

- [1] E. Yilmaz, Advances in reducing large volumes of environmentally harmful mine waste rocks and tailings, *Mineral Resources Management* 27 (2) (2011) 89–112.
- [2] G.M. Mudd, D.V. Boger, The ever-growing case for paste and thickened tailings – towards more sustainable mine waste management, *The AusIMM Bulletin* 2 (2013) 56–59.
- [3] R. Sairinen, H. Tiainen, T. Mononen, Talvivaara mine and water pollution: an analysis of mining conflict in Finland, *The Extractive Industries and Society* 4 (3) (2017) 640–651.
- [4] B. Koohestani, A.K. Darban, E. Darezereshki, P. Mokhtari, E. Yilmaz, E. Yilmaz, The influence of sodium and sulfate ions on total solidification and encapsulation potential of iron-rich acid mine drainage in silica gel, *Journal of Environmental Chemical Engineering* 6 (2) (2018) 3520–3527.
- [5] W.B. Zhu, J.M. Xu, J.L. Xu, D.Y. Chen, J.X. Shi, Pier-column backfill mining technology for controlling surface subsidence, *Int. J. Rock Mech. Min. Sci.* 96 (2017) 58–65.
- [6] H. Jiang, M. Fall, E. Yilmaz, L. Yang, L. Ren, Effect of mineral admixtures on flow properties of fresh cemented paste backfill: assessment of time dependency and thixotropy, *Powder Technol.* 372 (2020) 258–266.
- [7] M. Edraki, T. Baumgart, E. Manlapig, D. Bradshaw, M. Franks, C.J. Moran, Designing mine tailings for better environmental, social and economic outcomes: a review of alternative approaches, *J. Clean. Prod.* 84 (2014) 411–420.
- [8] M. Fall, J.C. Célestine, M. Pokharel, M. Touré, A contribution to understanding the effects of curing temperature on mechanical properties of cemented tailings backfill, *Eng. Geol.* 114 (2010) 397–413.
- [9] E. Yilmaz, T. Belem, M. Benzaazoua, One-dimensional consolidation parameters of cemented paste backfill, *Mineral Resources Management* 28 (4) (2012) 29–45.
- [10] Y.Y. Tan, D. Elmo, Y.C. Zhou, W.D. Song, X. Meng, Long-term mechanical behavior and characteristics of cemented tailings backfill through impact loading, *International Journal of Minerals, Metallurgy and Materials* 2 (27) (2020) 140–152.
- [11] E. Yilmaz, T. Belem, M. Benzaazoua, Study of physico-chemical and mechanical characteristics of consolidated and unconsolidated cemented paste backfills, *Mineral Resources Management* 29 (2013) 81–100.
- [12] J.Y. Wu, M.M. Feng, X.B. Mao, J.M. Xu, W.L. Zhang, X.Y. Ni, G.S. Han, Particle size distribution of aggregate effects on mechanical and structural properties of cemented rock fill: experiments and modelling, *Construct. Build. Mater.* 193 (2018) 295–311.
- [13] S. Cao, E. Yilmaz, G. Xue, W. Song, Assessment of acoustic emission and triaxial mechanical strength properties of rock-cemented tailings matrix composites, *Advances in Materials Science and Engineering* 6742392 (2019) 12, <https://doi.org/10.1155/2019/6742392>.

- [14] L. Yang, W. Xu, E. Yilmaz, Q. Wang, J. Qiu, A combined experimental and numerical study on the triaxial and dynamic compression behavior of cemented tailings backfill, *Eng. Struct.* 219 (2020) 110957.
- [15] C.C. Qi, A. Fourie, Cemented paste backfill for mineral tailings management: review and future perspectives, *Miner. Eng.* 144 (2019) 106025.
- [16] I. Alp, H. Deveci, Y.H. Sungun, A.O. Yilmaz, A. Kesimal, E. Yilmaz, Pozzolanic characteristics of a natural raw material for use in blended cements, *Iran. J. Sci. Technol. Trans. B-Eng.* 33 (B4) (2009) 291–300.
- [17] L. Cui, M. Fall, Multiphysics modelling and simulation of strength development and distribution in cemented tailings backfill structures, *International Journal of Concrete Structures and Materials* 12 (2018) 25, <https://doi.org/10.1186/s40069-018-0250-y>.
- [18] E. Yilmaz, T. Belem, B. Bussiere, M. Benzaazoua, Relationships between microstructural properties and compressive strength of consolidated and unconsolidated cemented paste backfills, *Cement Concr. Compos.* 33 (6) (2011) 702–715.
- [19] S. Cao, E. Yilmaz, G. Xue, E. Yilmaz, W. Song, Loading rate effect on uniaxial compressive strength behavior and acoustic emission properties of cemented tailings backfill, *Construct. Build. Mater.* 213 (2019) 313–324.
- [20] Y. Wang, M. Fall, A. Wu, Initial temperature-dependence of strength development and self-desiccation in cemented paste backfill that contains sodium silicate, *Cement Concr. Compos.* 67 (2016) 101–110.
- [21] D. Wu, R. Zhao, W. Hou, S. Wang, A coupled thermo-mechanical damage modeling application of cemented coal gangue-fly ash backfill under uniaxial compression, *Arabian J. Sci. Eng.* 45 (2020) 3469–3478.
- [22] G. Xue, E. Yilmaz, W. Song, S. Cao, Fiber length effect on strength properties of polypropylene fiber reinforced cemented tailings backfill specimens with different sizes, *Construct. Build. Mater.* 241 (2020) 118113.
- [23] D. Wu, R.K. Zhao, C.W. Xie, S. Liu, Effect of curing humidity on performance of cemented paste backfill, *International Journal of Minerals, Metallurgy and Materials* 27 (8) (2020) 1046–1053.
- [24] M. Benzaazoua, T. Belem, E. Yilmaz, Novel lab tool for paste backfill, *Can. Min. J.* 127 (3) (2016) 31–33.
- [25] L. Yang, W. Xu, E. Yilmaz, Q. Wang, J. Qiu, A combined experimental and numerical study on the triaxial and dynamic compression behavior of cemented tailings backfill, *Eng. Struct.* 219 (2020) 110957.
- [26] B. Koohestani, A.K. Darban, P. Mokhtari, E. Darezeshki, E. Yilmaz, E. Yilmaz, Influence of hydrofluoric acid leaching and roasting on mineralogical phase transformation of pyrite in sulfidic mine tailings, *Minerals* 10 (6) (2020) 513.
- [27] B. Yan, W. Zhu, C. Hou, E. Yilmaz, M. Saadat, Characterization of early age behavior of cemented paste backfill through the magnitude and frequency spectrum of ultrasonic P-wave, *Construct. Build. Mater.* 249 (2020) 118733.
- [28] R. Dandautiya, A.P. Singh, Utilization potential of fly ash and copper tailings in concrete as partial replacement of cement along with life cycle assessment, *Waste Manag.* 99 (2019) 90–101.
- [29] W.B. Xu, Y. Cao, B.H. Liu, Strength efficiency evaluation of cemented tailings backfill with different stratified structures, *Eng. Struct.* 180 (2019) 18–28.
- [30] S. Cao, G. Xue, E. Yilmaz, Y. Zhenyu, Y. Fudou, Utilizing concrete pillars as an environmental mining practice in underground mines, *J. Clean. Prod.* 278 (2021) 123433.
- [31] D.-Y. Yoo, N. Banthia, Impact resistance of fiber-reinforced concrete – a review, *Cement Concr. Compos.* 104 (2019) 103389.
- [32] L. Festugato, A. Peccin da Silva, A. Diambra, N.C. Consoli, E. Ibrahim, Modelling tensile/compressive strength ratio of fibre reinforced cemented soils, *Geotext. Geomembranes* 46 (2) (2018) 155–165.
- [33] J.-Y. Wang, N. Banthia, M.-H. Zhang, Effect of shrinkage reducing admixture on flexural behaviors of fibre reinforced cementitious composites, *Cement Concr. Compos.* 34 (4) (2012) 443–450.
- [34] N.C. Consoli, M.A.A. Bassani, L. Festugato, Effect of fiber-reinforcement on the strength of cemented soils, *Geotext. Geomembranes* 28 (4) (2010) 344–351.
- [35] R.J. Mitchell, D.M. Stone, Stability of reinforced cemented backfills, *Can. Geotech. J.* 24 (2) (1987) 189–197.
- [36] N.C. Consoli, H.P. Nierwinski, A. Peccin da Silva, J. Sosnoski, Durability and strength of fiber reinforced compacted gold tailings-cement blends, *Geotext. Geomembranes* 45 (2) (2017) 98–102.
- [37] X. Chen, X. Shi, J. Zhou, Q. Chen, E. Li, X. Du, Compressive behavior and microstructural properties of tailings polypropylene fibre-reinforced cemented paste backfill, *Construct. Build. Mater.* 190 (2018) 211–221.
- [38] X.W. Yi, G.W. Ma, A. Fourie, Centrifuge model studies on the stability of fibre-reinforced cemented paste backfill stopes, *Geotext. Geomembranes* 46 (2018) 396–401.
- [39] G. Xue, E. Yilmaz, W. Song, E. Yilmaz, Influence of fiber reinforcement on mechanical behavior and microstructural properties of cemented tailings backfill, *Construct. Build. Mater.* 213 (2019) 275–285.
- [40] G. Xue, E. Yilmaz, W. Song, S. Cao, Mechanical, flexural and microstructural properties of cement-tailings matrix composites: effect of fiber type and dosage, *Compos. B Eng.* 172 (2019) 131–142.
- [41] W. Xu, Q. Li, Y. Zhang, Influence of temperature on compressive strength, microstructure properties and failure pattern of fiber-reinforced cemented tailings backfill, *Construct. Build. Mater.* 222 (2019) 776–785.
- [42] X. Chen, X. Shi, J. Zhou, Z. Yu, Influence of polypropylene fiber reinforcement on tensile behavior and failure mode of tailings cemented paste backfill, *IEEE Access* 7 (2019) 69015–69026.
- [43] X. Chen, X. Shi, S. Zhang, H. Chen, J. Zhou, Z. Yu, P. Huang, Fiber-reinforced cemented paste backfill: the effect of fiber on strength properties and estimation of strength using nonlinear models, *Materials* 13 (2020) 718.
- [44] S. Cao, E. Yilmaz, W.D. Song, Fiber type effect on strength, toughness and microstructure of early age cemented tailings backfill, *Construct. Build. Mater.* 223 (2019) 44–54.
- [45] S. Cao, G. Xue, E. Yilmaz, Flexural behavior of fiber reinforced cemented tailings backfill under three-point bending, *IEEE Access* 7 (2019) 139317–139328.
- [46] B. Koohestani, A.K. Darban, P. Mokhtari, E. Yilmaz, E. Darezeshki, Comparison of different natural fibers treatments – a literature review, *Int. J. Environ. Sci. Technol.* 16 (1) (2019) 629–642.
- [47] X. Xu, M. Fall, I. Alainachi, K. Fang, Characterisation of fibre-reinforced backfill/rock interface through direct shear tests, *Geotechnical Research* 7 (1) (2020) 11–25.
- [48] Y.P. Kou, H.Q. Jiang, L. Ren, E. Yilmaz, Y.H. Li, Rheological properties of cemented paste backfill with alkali-activated slag, *Minerals* 10 (3) (2019) 288.
- [49] M. Pokharel, M. Fall, Combined influence of sulphate and temperature on the saturated hydraulic conductivity of hardened cemented paste backfill, *Cement Concr. Compos.* 38 (2013) 21–28.
- [50] R. Ranade, M.D. Stults, V.C. Li, T.S. Rushing, J. Ronth, W.F. Heard, Development of high strength high ductility concrete, 2nd Int. RILEM Conference on Strain Hardening Cementitious Composites (2011) 1–8.
- [51] R. Shahrin, C.P. Bobko, Micropillar compression investigation of size effect on microscale strength and failure mechanism of Calcium-Silicate-Hydrates (C-S-H) in cement paste, *Cement Concr. Res.* 125 (2019) 105863.
- [52] J. Tatar, C.R. Taylor, H.R. Hamilton, A multiscale micromechanical model of adhesive interphase between cement paste and epoxy supported by nanomechanical evidence, *Compos. B Eng.* 172 (2019) 679–689.
- [53] Y.L. Ji, L. Pel, Z.P. Sun, The microstructure development during bleeding of cement paste: an NMR study, *Cement Concr. Res.* 125 (2019) 105866.
- [54] J.Y. Wu, M.M. Feng, X.Y. Ni, X.B. Mao, Z.Q. Chen, G.S. Han, Aggregate gradation effects on dilatancy behavior and acoustic characteristic of cemented rock fill, *Ultrasonics* 92 (2019) 79–92.
- [55] L. Assi, V. Soltangharai, R. Anay, P. Ziehl, F. Matta, Unsupervised and supervised pattern recognition of acoustic emission signals during early hydration of Portland cement paste, *Cement Concr. Res.* 103 (2018) 216–225.
- [56] D. Wu, Y.L. Zhang, Y.C. Liu, Mechanical performance and ultrasonic properties of cemented gangue backfill with admixture of fly ash, *Ultrasonics* 64 (2016) 89–96.
- [57] S. Cao, W.D. Song, Effect of filling interval time on the mechanical strength and ultrasonic properties of cemented coarse tailings backfill, *Int. J. Miner. Process.* 166 (2017) 62–68.
- [58] G. Xue, E. Yilmaz, W. Song, S. Cao, Analysis of internal structure behavior of fiber reinforced cement-tailings matrix composites through X-ray computed tomography, *Compos. B Eng.* 175 (2019) 107091.
- [59] W. Sun, K.P. Hou, Z.Q. Yang, Y.M. Wen, X-ray CT three-dimensional reconstruction and discrete element analysis of the cement paste backfill pore structure under uniaxial compression, *Construct. Build. Mater.* 138 (2017) 69–78.
- [60] S.H. Cho, M. Yokota, M. Ito, S. Kawasaki, S.B. Jeong, B.K. Kim, K. Kaneko, Electrical disintegration and micro-focus X-ray CT observations of cement paste samples with dispersed mineral particles, *Miner. Eng.* 57 (2014) 79–85.
- [61] R. Griffiths, A. Ball, An assessment of the properties and degradation behaviour of glass-fibre-reinforced polyester polymer concrete, *Compos. Sci. Technol.* 60 (14) (2000) 2747–2753.
- [62] Q. Zeng, Z. Lin, C.S. Zhou, J.Y. Wang, Capillary imbibition of ethanol in cement paste traced by X-ray computed tomography with CsCl-enhancing technique, *Chem. Phys. Lett.* 726 (2019) 117–123.
- [63] J.S. Kim, L.H. Kim, T.S. Han, Microstructure characterization of cement paste from micro-CT and correlations with mechanical properties evaluated from virtual and real experiments, *Mater. Char.* 155 (2019) 109807.
- [64] J.S. Kim, S.Y. Chung, D. Stephan, T.S. Han, Issues on characterization of cement paste microstructures from μ -CT and virtual experiment framework for evaluating mechanical properties, *Construct. Build. Mater.* 202 (2019) 82–102.
- [65] P. Wang, Z. Karatza, C. Arson, DEM modelling of sequential fragmentation of zeolite granules under oedometric compression based on XCT observations, *Powder Technol.* 347 (2019) 66–75.
- [66] T.S. Han, X.X. Zhang, J.S. Kim, S.Y. Chung, J.H. Lim, C. Linder, Area of lineal-path function for describing the pore microstructures of cement paste and their relations to the mechanical properties simulated from μ -CT microstructures, *Cement Concr. Compos.* 89 (2018) 1–17.
- [67] D.C. González, J. Mínguez, M.A. Vicente, F. Cambronero, G. Aragon, Study of the effect of the fibers' orientation on the post-cracking behavior of steel fiber reinforced concrete from wedge-splitting tests and computed tomography scanning, *Construct. Build. Mater.* 192 (2018) 110–122.
- [68] S.Y. Chung, T.S. Han, S.Y. Kim, Reconstruction and evaluation of the air permeability of a cement paste specimen with a void distribution gradient using CT images and numerical methods, *Construct. Build. Mater.* 87 (2015) 45–53.
- [69] T. Mishurova, N. Rachmatulin, P. Fontana, T. Oesch, G. Bruno, E. Radi, I. Sevostianov, Evaluation of the probability density of inhomogeneous fiber orientations by computed tomography and its application to the calculation of the effective properties of a fiber-reinforced composite, *Int. J. Eng. Sci.* 122 (2018) 14–29.
- [70] Y.G. Yang, Y.S. Zhang, W. She, Z. Wu, Z.Y. Liu, Y.J. Ding, Nondestructive monitoring the deterioration process of cement paste exposed to sodium sulfate solution by X-ray computed tomography, *Construct. Build. Mater.* 186 (2018) 182–190.
- [71] D. Asahina, E.N. Landis, J.E. Bolander, Modeling of phase interfaces during pre-critical crack growth in concrete, *Cement Concr. Compos.* 33 (9) (2011) 966–977.

- [72] P.H.R. Borges, N. Banthia, H.A. Alcamand, W.L. Vasconcelos, E.H.M. Nunes, Performance of blended metakaolin/blastfurnace slag alkali-activated mortars, *Cement Concr. Compos.* 71 (2016) 42–52.
- [73] M.A. Vicente, G. Ruiz, D.C. González, J. Mínguez, M. Tarifa, X. Zhang, CT-Scan study of crack patterns of fiber-reinforced concrete loaded monotonically and under low-cycle fatigue, *Int. J. Fatig.* 114 (2018) 138–147.
- [74] D.F. McCarthy, *Essentials of Soil Mechanics and Foundations: Basic Geotechnics*, seventh ed., Pearson Prentice Hall, Toronto, Canada, 2007, pp. 1–864.
- [75] D. Landriault, *Backfill in Underground Mines – Underground Mining Methods Engineering Fundamentals and International Case Studies*, United States, Society for Mining, Metallurgy & Exploration, Littleton, Colorado, 2001, pp. 601–614 (Chapter 69).
- [76] ASTM C1116/C1116M-10a, Standard Specification for Fiber-Reinforced Concrete, ASTM International, West Conshohocken, PA, 2015. www.astm.org.
- [77] ACI 544.3R-08. Guide for Specifying, Proportioning, and Production of Fiber-Reinforced Concrete, American Concrete Institute (ACI), Farmington Hills, MI, 2008. www.concrete.org.
- [78] ASTM C94/C94M-20, Standard Specification for Ready-Mixed Concrete, ASTM International, West Conshohocken, PA, 2020. www.astm.org.
- [79] ASTM C39/C39M-18, Standard Method for Compressive Strength of Cylindrical Concrete Specimens, ASTM International, West Conshohocken, PA, 2001. www.astm.org.
- [80] T. Nguyen, A. Ghazlan, A. Kashani, S. Bordas, T. Ngo, 3D meso-scale modelling of foamed concrete based on X-ray Computed Tomography, *Construct. Build. Mater.* 188 (2018) 583–598.
- [81] Y.J. Zhao, X.W. Wang, J.W. Jiang, L. Zhou, Characterization of interconnectivity, size distribution and uniformity of air voids in porous asphalt concrete using X-ray CT scanning images, *Construct. Build. Mater.* 213 (2019) 182–193.
- [82] J.B. Zhu, T. Zhou, Z.Y. Liao, L. Sun, X.B. Li, R. Chen, Replication of internal defects and investigation of mechanical and fracture behaviour of rock using 3D printing and 3D numerical methods in combination with X-ray computerized tomography, *Int. J. Rock Mech. Min. Sci.* 106 (2018) 198–212.
- [83] N. Banthia, F. Majdzadeh, J. Wu, V. Bindiganavile, Fiber synergy in hybrid fiber reinforced concrete (HyFRC) in flexure and direct shear, *Cement Concr. Compos.* 48 (2014) 91–97.
- [84] S. Cao, D. Zheng, E. Yilmaz, Z.Y. Yin, G.L. Xue, F.D. Yang, Strength development and microstructure characteristics of artificial concrete pillar considering fiber type and content effects, *Construct. Build. Mater.* 256 (2020) 119408.
- [85] P. Sheng, J. Zhang, Z. Ji, An advanced 3D modeling method for concrete-like particle-reinforced composites with high volume fraction of randomly distributed particles, *Compos. Sci. Technol.* 134 (2016) 26–35.
- [86] F. Yu, D.Q. Sun, M.J. Hu, J. Wang, Study on the pores characteristics and permeability simulation of pervious concrete based on 2D/3D CT images, *Construct. Build. Mater.* 200 (2019) 687–702.
- [87] Y. Wang, H.J. Wang, X.L. Zhou, X.F. Yi, Y.G. Xiao, X.M. Wei, In situ X-ray CT investigations of meso-damage evolution of cemented waste rock-tailings backfill (CWRTB) during triaxial deformation, *Minerals* 9 (1) (2019) 52.
- [88] H.Q. Jiang, H. Yi, E. Yilmaz, S. Liu, J. Qiu, Ultrasonic evaluation of strength properties of cemented paste backfill: effects of mineral admixture and curing temperature, *Ultrasonics* 100 (2020) 105983.
- [89] L. Zhang, Q.P. Wei, J.J. An, L. Ma, K.C. Zhou, W.T. Ye, Z.M. Yu, X.P. Gan, C.T. Lin, J.T. Luo, Construction of 3D interconnected diamond networks in Al-matrix composite for high-efficiency thermal management, *Chem. Eng. J.* 380 (2020) 122551.
- [90] R. Yu, P. Spiesz, H.J.H. Brouwers, Energy absorption capacity of a sustainable Ultra-High Performance Fibre Reinforced Concrete (UHPFRC) in quasi-static mode and under high velocity projectile impact, *Cement Concr. Compos.* 68 (2016) 109–122.
- [91] N. Banthia, N. Nandakumar, Crack growth resistance of hybrid fiber reinforced cement composites, *Cement Concr. Compos.* 25 (1) (2003) 3–9.
- [92] L. Li, M.L. Cao, X. Ming, H. Yin, Y.N. Sun, Microstructure of calcium carbonate whisker reinforced cemented paste after elevated temperature exposure, *Construct. Build. Mater.* 227 (2019) 116609.
- [93] S. Cao, E. Yilmaz, W.D. Song, Dynamic response of cement-tailings matrix composites under SHPB compression load, *Construct. Build. Mater.* 186 (2018) 892–903.
- [94] F. Shi, T.M. Pham, R. Hao, Y.F. Hao, Post-cracking behavior of basalt and macro polypropylene hybrid fibre reinforced concrete with different compressive strengths, *Construct. Build. Mater.* 262 (2020) 120108.
- [95] N. Banthia, F. Majdzadeh, J. Wu, V. Bindiganavile, Fiber synergy in hybrid fiber reinforced concrete (HyFRC) in flexure and direct shear, *Cement Concr. Compos.* 48 (2014) 91–97.